Dalton Transactions

PAPER

View Article Online
View Journal | View Issue

Cite this: *Dalton Trans.*, 2015, **44**, 13315

Received 25th March 2015,
Accepted 15th June 2015

DOI: 10.1039/c5dt01178g

www.rsc.org/dalton

Binuclear complexes of Ni(I) from 4-terphenyldithiophenol†

Felix Koch, Hartmut Schubert, Peter Sirsch and Andreas Berkefeld*

Binuclear complexes of Ni(I) have been prepared from a 4-terphenyldithiophenol ligand. Steric effects were found to determine the formation of coordination isomeric structures that differ in the nature of metal-to-ligand bonding. Coordination of spatially demanding phosphine ligands PR_3, R = C_6H_6, C_6H_{11}, at nickel sites results in a butterfly shaped thiolate-bridged $Ni_2(\mu\text{-}S)_2$ motif. For smaller PMe_3, the central π-system of the 4-terphenyl backbone adopts a bis-allyl like μ-*syn*-η^3:η^3-C_6H_4 structure due to significant d-π* Ni(I)-to-ligand charge transfer. Delocalisation indices δ(Ni–Ni) derived from DFT calculations provide a metric to assess the strength of electronic coupling of the Ni sites based on solid state structural data, and indicated less strong electronic coupling for the bis-allyl like structure with δ(Ni–Ni) = 0.225 as compared to 0.548 for the $Ni_2(\mu\text{-}S)_2$ structural motif. A qualitative reactivity study toward $CNCH_3$ as an auxiliary ligand has provided the first insight into the chemical properties of the bimetallic complexes presented.

Introduction

The class of binuclear complexes of Ni(I) features a remarkable structural diversity, and the ligand design plays a pivotal role in this regard. One can differentiate between structural motifs in which electronic coupling of the Ni(I) ions either occurs through bonding to (i) bridging conjugated π-systems in both *syn*- and antarafacial fashion,[1–8] (ii) bridging amido,[9] phosphido,[10] thiolato,[11,12] sulfido,[13] halogenido,[14–17] and hydrido[18] ligands in the form of $Ni_2(\mu\text{-}X)_2$ cores, (iii) bridging diphosphine,[19,20] and biphenyldiyl[15,21,22] ligands, or in the form of unsupported Ni–Ni bonds.[23–25] Antiferromagnetic coupling through a ligand and direct Ni–Ni bonding results in diamagnetic behaviour in most instances, albeit triplet ground states have been proposed for the $Ni_2(\mu\text{-}Br)_2$ core bound to the neutral form of a redox active 1,8-naphthyridine diimine ligand.[16]

Based on solution reactivity and VT EPR studies on solid samples dinickel biradicals coexist in thermal equilibria with diamagnetic ground states. In the biradical state the Ni–Ni interaction is non-bonding and dissociation is a favourable and facile process.[2,5,9] The reversible formation of reactive Ni(I) species appears to represent one of the two major modes of reactivity displayed by binuclear Ni(I) complexes. An early example of binuclear reactivity is the tetramerisation of ethyne to cyclooctatetraene as put forward by Wilke.[26] Despite the exact mechanism of this process remaining unresolved, dinickel(I) complexes have been reported to catalyse reductive C–C bond formation in a cooperative fashion,[15,21,22] to act as precursors in bimetallic catalytic group transfer reactions to form carbodiimides and isocyanates,[17,27] and to activate secondary silanes for the catalytic hydrosilation of unsaturated substrates.[28]

The capability of thiolate ligands to bridge a pair of metals through bis-μ-thiolate coordination aids the formation of binuclear and higher nuclearity complexes,[29–33] including well characterised examples for Ni(I) of type **I** in Scheme 1.[10–12] In the context of a reactivity study of thiolate complexes of Ni(I), Tatsumi and co-workers reported the structure of a binuclear Ni(I) complex with bridging arene and thiolate groups, see **II** in Scheme 1.[11]

We have set out to develop the coordination chemistry of binucleating terphenyldithiophenol ligands which combine the properties of metal–sulphur[34,35] and labile metal–arene[36]

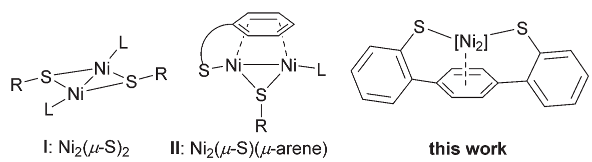

Scheme 1 General structural motifs of dinuclear Ni(I) complexes with L = neutral ligand, *e.g. tert*-phosphine, NHC, and R = aryl, *tert*-alkyl, H.

*Institut für Anorganische Chemie, Eberhard Karls Universität Tübingen, Auf der Morgenstelle 18, 72076 Tübingen, Germany.
E-mail: andreas.berkefeld@anorg.uni-tuebingen.de; Tel: +49 7071 29 76213*

† Electronic supplementary information (ESI) available: Additional computational, experimental, and NMR spectroscopic details. CCDC 1042645 (**1**), 1042646 (**2**), 1042647 (**3**), 1042648 (**4**), and 1042649 (**5**). For ESI and crystallographic data in CIF or other electronic format see DOI: 10.1039/c5dt01178g

bonds. The use of a dianionic ligand framework eliminates the necessity for incorporating secondary anionic ligands that might bridge the nickel ions, which may provide structural flexibility to the bimetallic core. Herein we report on the synthesis and properties of mono- and binuclear complexes of nickel with such a type of ligand.

Results and discussion

Synthesis and structure of mono- and binuclear complexes 1–5

The preparation of the nickel complexes followed two different protocols. The first utilises the comproportionation of Ni(II) precursors **1** and **2** with Ni(COD)$_2$, COD being 1,5-cyclooctadiene. Alternatively, reacting 4-terphenyldithiophenol with 2 equiv. of $(PPh_3)_2NiN(SiMe_3)_2$ as a source of Ni(I) affords bimetallic **5** directly, eliminating bis(trimethylsily)amine and PPh_3.[11]

Ni(II) precursor complexes **1** or **2** have been prepared by salt metathesis, with a reaction of the dipotassium salt of dithiophenol with Ni(II) chloride precursors in toluene solution at ambient temperature as shown in Scheme 2. The compounds have been isolated as purple solids in yields of 88 and 60% with λ_{max}(thf) for **1** at 511 (ε/dm^3 mol^{-1} cm^{-1} 1128) and **2** at 550 (3545) nm. Note that **2** is a kinetic reaction product and was found to gradually convert into an unknown red precipitate, most likely an oligomeric composition. Substituting PCy_3 for PPh_3 affords a mixture of ill-defined products.

Single crystal XRD structural analysis verified square planar coordination geometries at the *trans*-dithiolatonickel(II) centres with average Ni–S bond lengths of 2.249(4) and 2.241(2) Å for **1** and **2** respectively which compare well with the Ni–S bond lengths reported for structurally related complexes.[10–12] The molecular structure of **2** is depicted in Fig. 1. While two PMe_3 donors complete the ligand shell of Ni(II) in **1**, the use of the more bulky PCy_3 ($\Delta\Theta_{Tolman}$ = 52°) ligand in **2** allows for binding just one phosphine ligand, with a Ni–P bond distance of 2.353(2) Å, and enforces η^2-coordination of the central aryl ring with an averaged Ni–C distance of 2.285(4) Å.

Also in the case of **1** the nickel ion resides above one of the C_2H_2 edges of the central arene ring, but the average Ni–C distance of 2.614(2) Å is significantly longer, as expected. The molecular structure of **1** is shown in Fig. S9, ESI.† Low-temperature $^{13}C\{^1H\}$ and ^1H NMR data are consistent with η^2-arene bonding to Ni(II) in **2**. At 193 K in d_2-CH_2Cl_2 solution, characteristic resonances of a C_s symmetric structure were observed at 108.4, broadened due to unresolved $^2J_{C-P}$ coupling, and 8.21 as well as 127.4 and 7.44 ppm which account for the Ni-bound and unbound, yet slowly exchanging C_2H_2 edges of the central aryl ring as defined in Scheme 2. At 298 K pseudo C_{2v} symmetric spectra result for both complexes with an *N*-line pattern at 0.77 ppm, $^{|2+4|}J_{H-P}$ = 7.8 Hz, for *trans*-$(Me_3P)_2$Ni(II) along with resonances of the nuclei at the central arene ring at 7.56 and 123.9 ppm for **1**, and at 7.76 and 118.6 ppm in the case of **2**.

Binuclear complexes **3–5** have been isolated in the form of distinct coordination isomers as depicted in Scheme 3 in yields of 51% (**3**, brown), 75% (**4**, yellow), and 73% (**5**, green) with λ_{max} (thf)/nm **3**, 520 (ε/dm^3 mol^{-1} cm^{-1} 2044), **4**, 352 (3005), and **5**, 450 (7821). Additional weak absorption bands

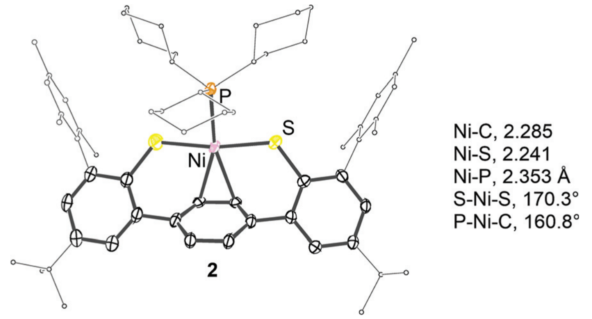

Fig. 1 ORTEP representation and selected structural parameters of the molecular structure of **2** (thermal ellipsoids at the 50% probability level). Given Ni–C, and –S distances are averaged, H- and lattice solvent atoms are not shown for clarity.

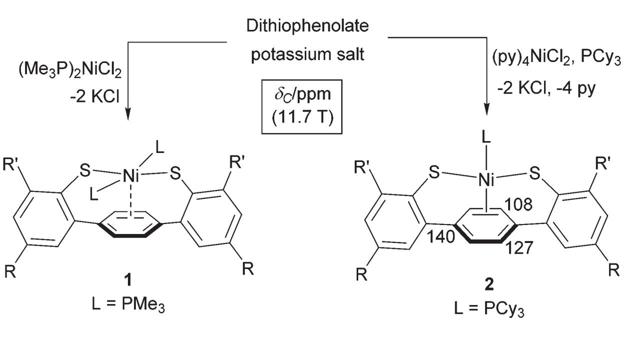

Scheme 2 Structure and characteristic δ_C (11.7 T) NMR chemical shifts of Ni(II) precursor complexes **1** and **2** (R′ = 2,4,6-$(H_3C)_3C_6H_2$, R = ^{t}Bu).

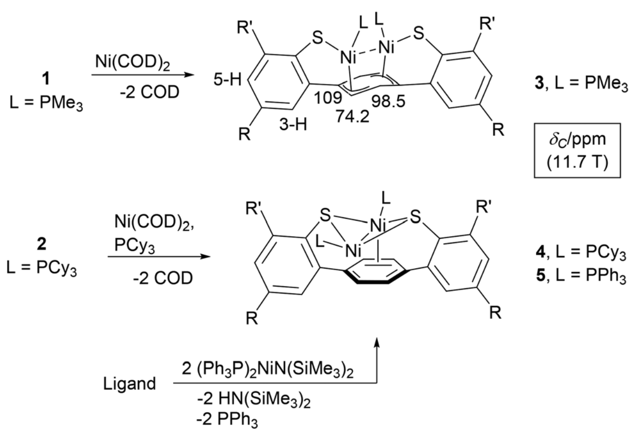

Scheme 3 Synthesis, structure, and characteristic δ_C (11.7 T) NMR chemical shifts of binuclear complexes **3–5** (R′ = 2,4,6-$(H_3C)_3C_6H_2$, R = ^{t}Bu).

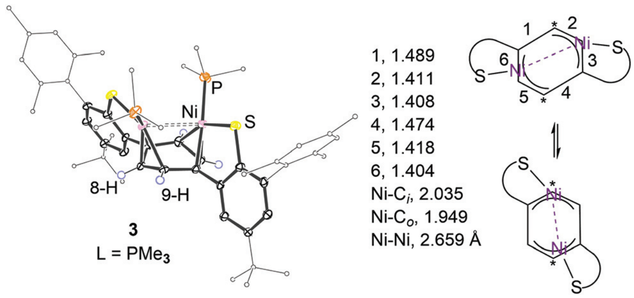

Fig. 2 Left: ORTEP representation and selected structural parameters of **3** (thermal ellipsoids at the 50% probability level; H- and lattice solvent atoms omitted for clarity). Right: schematic representation of the overall exchange process of the Ni(I)$_2$ fragment (as a visual aid, asterisks highlight identical C atoms).

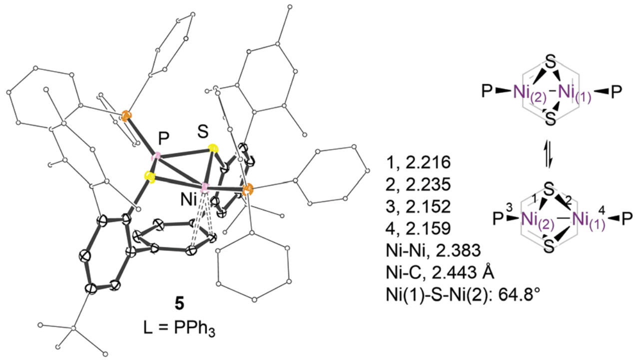

Fig. 3 ORTEP representation and selected structural parameters of **5** (thermal ellipsoids at the 50% probability level; H- and lattice solvent atoms omitted for clarity), and schematic representation of a seesaw-like motion of the $Ni_2(\mu\text{-}S)_2$ fragment.

were detected for each of the dinickel complexes at wavelengths of 940–990 nm (ε/dm^3 mol^{-1} cm^{-1} 200–500).

Single crystal XRD structure analysis verified the binding modes of the dinickel cores to the dithiophenolate ligand as exemplified for **3** and **5** in Fig. 2 and 3. A distinct structural feature of **3** is the boat shaped conformation of the central π-system which is present in both the solid state and solution. The variation of bond lengths and deformation from planarity indicate the formation of a *syn*-μ-η^3:η^3 bonding motif, which likely results from a significant overlap of the occupied d-orbitals at both nickel ions with a π*-orbital of the arene π-system.[36–38] Short distances of 1.949(4), 2.035(4), and 2.149(4) Å between Ni and *o*-, i-, and *m*-C atoms, and a long Ni–Ni separation of 2.659(1) Å support this description. The observed κ^1-S–Ni bond lengths of 2.205(1) and 2.193(3) Å compare well with those in the literature.[11] Such tight Ni$_2$-arene bonding is likely a consequence of a strong charge donation from the thiolate and phosphine ligands to nickel. A structurally similar conformation was reported for the central π-system of a 4-terphenyl-diphosphine ligand that stabilises a bridging μ-η^1:η^1-*o*,*o*′-biphenyldiyl dinickel fragment.[15]

The geometry at each Ni ion may be best described as a distorted square planar defined by the sulphur, phosphorus, and the peripheral C-atoms of the η^3-allyl moiety. The shortest distance between hydrogen atoms at the PMe$_3$ ligands is 2.5 Å.

The dinickel core of **3** is dynamic. For an 11.7 T magnetic field, the resonance at δ_H 5.41 ppm of protons 8/9-H at the central π-system was observed to coalesce at 203 K. Further cooling to 178 K gave rise to broad ^{1}H and ^{13}C NMR resonances at 4.97 ($\nu_{1/2} \sim 26$ Hz) and 5.59 ($\nu_{1/2} \sim 23$ Hz) as well as 109 (i-C, $\nu_{1/2} \sim 42$ Hz), 74.2 (*o*-C, $\nu_{1/2} \sim 60$ Hz), and 98.5 (*m*-C, $\nu_{1/2} \sim 55$ Hz) ppm. Exchange cross peaks between protons 8/9-H are well established in ^{1}H–^{1}H NOESY data at 178 K. Apparent exchange of 8-H for 9-H requires the Ni(I) ions to formally change sites across the *syn*-μ-η^3:η^3-C_6H_4 system as schematised in Fig. 2. Whether this process evolves through an intermediate structure analogous to that of **4** and **5** is unknown.

Steric interactions between the mesityl and phosphine substituents in **4** and **5** impair a close approach of both nickel ions to the arene system. Instead, the $P_{(1)}$–$Ni_{(1)}$–$Ni_{(2)}$–$P_{(2)}$ moiety is tilted upward relative to the aryl ring plane which allows one nickel ion, $Ni_{(1)}$, to weakly interact with the undistorted π-system as indicated in Fig. 3.

The observed average $Ni_{(1)}$–C distances of 2.569(6) and 2.443(1)[39] Å in **4** and **5** respectively are significantly longer than those found in **2** (2.285(4) Å). The formation of a *syn-endo*-$Ni_2(\mu\text{-}S)_2$ structure[29] compensates for the lack of metal–arene interactions at $Ni_{(2)}$. As a result, slightly shorter average μ-S–$Ni_{(2)}$ and $Ni_{(2)}$–P bond distances of 2.213(1) ($\Delta d = 0.02$) and 2.148(1) ($\Delta d = 0.009$) Å as compared to the respective bonds to $Ni_{(1)}$ have been found. Acute $Ni_{(1)}$–S–$Ni_{(2)}$ angles of 65° within the $Ni_2(\mu\text{-}S)_2$ entity are accompanied by a short Ni–Ni separation of 2.383(1) Å.[10,11,29]

Exchange averaged singlet ^{1}H NMR resonances of the C_2H_2 moieties of the central aryl rings in **4** and **5** have been observed at 8.41 ($\nu_{1/2} \sim 95$ Hz) and 7.72 ($\nu_{1/2} \sim 33$ Hz) ppm at 168 K. Whether or not this exchange involves preliminary dissociation of one phosphine ligand is unclear albeit no spectral differences have been observed in the presence of excess (≤5%) phosphine. As for **3**, the apparent exchange of the C_2H_2 sites requires an overall seesaw-like motion as schematised in Fig. 3.

Computational study

A comparison of Ni–Ni and Ni–C(arene) bond lengths calculated from single crystal X-ray diffraction data suggests a higher contribution of direct metal–metal (M–M) bonding to the coupling of the nickel ions in the case of the *syn-endo*-$Ni_2(\mu\text{-}S)_2$ structural motif in **4** and **5** than in **3**. To gain deeper insight into the nature and actual strength of Ni–Ni bonding in these structurally different complexes, we carried out a topological analysis of their electron density distribution, $\rho(\mathbf{r})$, as derived from the DFT calculations of **3** and **5**, using the "quantum theory of atoms in molecules" (QTAIM) approach.[40,41] DFT calculations were performed using Gaussian[42] at the B3LYP/6-311G(d,p) level[43–49] with dispersion corrections, including Becke–Johnson damping,[50,51] and substituting the ^{t}Bu groups on the ligand for CH_3 in the theoretical model systems. The optimised geometries were in excellent agreement with the experimental counterparts, and the Ni–Ni distances differed by 2 and 6.1 pm for **3** and **5**, respectively. For computational details and the full geometries, see the ESI.†

Although numerous experimental and theoretical electron density studies on M–M bonding in dinuclear complexes have been reported, a fundamental understanding of this interaction remains elusive.[52,53] In both **3** and **5**, a stable bond path[54] between the two nickel ions could be identified which implies direct M–M interactions in both systems. This observation is noteworthy, as the presence of bridging ligands usually results in the loss of M–M bond paths, in particular for metal atoms linked by formal single bonds, as concluded by Farrugia and Macchi in a recent review.[53] The topological parameters of $\rho(\mathbf{r})$ at the Ni–Ni bond critical points (BCPs)[55] in **3** and **5** are listed in Table 1, and the extended topological data and the molecular graphs of **3** and **5** are provided in the ESI.† In both systems, the value for $\rho(\mathbf{r}_b)$ is relatively small, a feature commonly observed for M–M bonds which has been attributed to the diffuse nature of this interaction.[53,56] The slightly negative values for the total energy density, $H(\mathbf{r}_b)$, imply that the potential energy density at these BCPs is somewhat larger than the kinetic energy density which is indicative of covalent bonding, despite the positive value for the Laplacian of $\rho(\mathbf{r}_b)$, $\nabla^2\rho(\mathbf{r}_b)$.[56,57] A better metric than $\rho(\mathbf{r}_b)$ to assess the actual strength of metal–metal bonding is provided by the delocalization index, δ(A–B), which measures the number of electron pairs shared between two atoms A and B, irrespective of the existing bond paths.[53,56,58] For **3** and **5**, the values of δ(Ni–Ni) are equal to 0.225 and 0.548, respectively. These smaller, fractional bond orders indicate what has been termed as a partial covalent character for formally M–M single bonds, in the sense that not a whole pair of electrons is involved in direct interactions between the atoms.[53] To summarise, the bonding between the Ni atoms in both **3** and **5** can be described as a combination of through-ligand and direct M–M bonding. The latter contribution was clearly identified through the existence of Ni–Ni bond paths. The large increase in the Ni–Ni separation by 27.6 pm [DFT: 31.7 pm] in **3** compared to **5** also reflects a significant reduction of Ni–Ni bond strength: the respective value of δ(Ni–Ni) in **5** is more than 2.4 times higher than the one in **3**, which can therefore be classified as a bimetallic complex exhibiting only very weak Ni–Ni interactions.

Table 1 Selected topological properties at the Ni–Ni bond critical points in the model systems of **3** and **5**

	d^a	$\rho(\mathbf{r}_b)^b$	$\nabla^2\rho(\mathbf{r}_b)^c$	ε	$G(\mathbf{r}_b)/\rho(\mathbf{r}_b)$	$H(\mathbf{r}_b)^d$
3	2.639	0.194	+1.856	0.02	0.879	−0.041
5	2.322	0.407	+1.686	0.36	0.674	−0.156

^{a} In units of Å. ^{b} In units of e Å^{-3}. ^{c} In units of e Å^{-5}. ^{d} In units of hartree Å^{-3}.

Solution properties of 3–5

VT ^{1}H NMR data of **3** and **5** revealed a marked dependence of chemical shifts and line-widths of specific proton resonances with temperature and solvent polarity. In the case of **3**, substituting the solvent d_8-thf with d_6-C_6H_6 at 299 K resulted in a $\Delta\delta_H$ of +1 ppm for protons 8/9-H at the central π-system. As shown in Fig. 4, variation of the temperature of a d_8-thf solution of **3** results in a reversible, non-linear variation of δ_H between 5.39 at 198 K and 11 ppm at 405 K, $\Delta\delta_H$(8/9-H) = 5.61 ppm.

In comparison, the observed chemical shift changes for the protons at the flanking phenyl rings, $\Delta\delta_H$(3-H) = 0.42, and 0.88 (5-H) ppm, and for the PMe_3 ligands (0.58 ppm) are smaller by about one order of magnitude but vary in the same non-linear fashion. The largest shift difference in the latter series accounts for the protons most distant from the nickel ions (5-H; for numbering *cf.* to Scheme 3) whereas resonances of the mesityl (26-H) and ^{t}Bu substituents are unaffected.

A similarly marked dependence emerged for **5** in d_8-thf with $\Delta\delta_H$(8,9-H) = 4.94 ppm and δ_H(8,9-H, 299 K) = 10.12 ppm (12.01 ppm in d_6-C_6H_6 and d_8-toluene) whereas it was found to be small in the case of **4**, with $\Delta\delta_H$(8,9-H) = 0.51 ppm and δ_H(8,9-H, 299 K) = 8.69 ppm. Plots of δ_H *vs.* temperature for selected types of protons for complexes **4** and **5** are provided in Fig. S7 and S8, ESI.† The respective values of δ_H and the variation in temperature have been observed for both raw products and single as well as double recrystallized samples of **3–5** that were obtained from different batches. This indicates that putative Ni(I) impurities most likely are not the reason for this solution behaviour.

Whereas the ^{1}H and ^{13}C NMR chemical shifts determined at low temperatures account for the respective structural features observed in the solid state structures of **3–5**, the continuous shift of δ_H to lower fields at higher temperatures, especially δ_H(8/9-H) being progressively greater than 11 ppm, suggests thermal population of a paramagnetic biradical (S = 1)

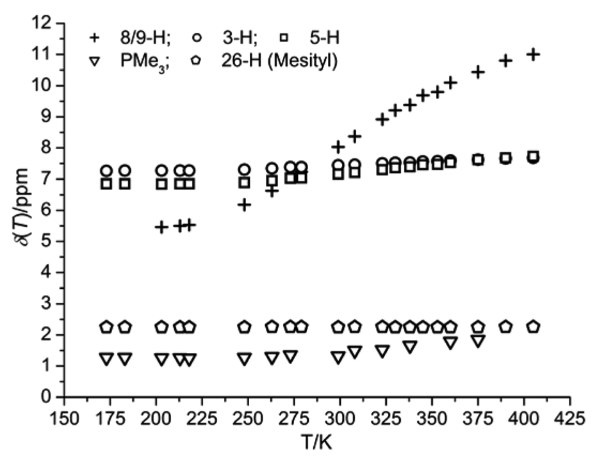

Fig. 4 Temperature dependence of δ_H observed for **3** (500 MHz, 21 mM in d_8-thf).

state[2,9] which would add contact and dipolar shift contributions to the observed chemical shift.[28,59,60] An independent parameter to probe for variable net electron spin moments is the trend of the temperature dependence of the ^{1}H spin–lattice relaxation time, T_1, which is expected to be positive for protons in diamagnetic environments. Values of T_1 for 8/9-H of **3–5** were found to decrease markedly with increasing temperatures, *e.g.* T_1(8/9-H) for **3** in d_8-thf decreased from 1300 ms at 223 K to 110 ms at 323 K; *cf.* to Fig. S3–S6, ESI.† Surprisingly, invariable effective magnetic moments of 0.9 B.M. for **3** and 1.0 B.M. for **5** in both toluene and thf solutions were determined by Evan's method[61,62] over the same temperature range at a field of 11.7 T. This finding challenges the hypothesis of the thermal equilibrium population of a paramagnetic spin state. Heating a solution of **5** in d_8-toluene to 373 K for 3 h was found to slightly increase the effective magnetic moment by ~0.1 B.M. but did not have any effect on the temperature dependence of δ_H.

Chemical properties of dinickel cores

Compounds **3–5** displayed appreciable thermal stability in VT NMR spectroscopic studies of their toluene and thf solutions. While heating a solution of **3** in d_6-benzene to 343 K for 2 h resulted in low conversion, ~3%, back into **1** no changes were observed in d_8-thf under identical conditions. When dissolved in d_2-CH_2Cl_2 under ambient conditions gradual deterioration to yet unknown products occurs in all cases. To gain a more detailed insight into the chemical properties of these bimetallic systems the reactivities of **3–5** were studied qualitatively toward methyl isocyanide ($CNCH_3$ = L′) by VT NMR spectroscopy.

^{1}H and ^{31}P NMR spectroscopic monitoring showed that **5** (δ_P 68 ppm) reacts with L′ in a 1 : 2 stoichiometry at $T \le 213$ K to produce a single product **5***2L′ with characteristic resonances δ_H(Ni–L′) 2.10 and δ_P 22.51 ppm as described in Scheme 4. Coordination of both PPh_3 and L′ to both Ni sites is supported by ^{1}H–^{1}H COSY and ^{1}H–^{31}P HSQC data which established the presence of scalar J_H and J_P coupling of the methyl protons of L′ with the *o*- and *m*-^{1}H and ^{31}P nuclei of coordinate PPh_3. Albeit we cannot assign a molecular structure based on the NMR data available, **5***2L′ must be a bimetallic complex. Warming the sample to 263 K in the NMR probe resulted in the progressive formation of $(Ph_3P)_2(L')_2$Ni(0) at the expense of the resonances of **5***2L′, with characteristic ^{1}H and ^{31}P NMR resonances at 2.85 ppm (*N*-line pattern, L′) and δ_P 33.2 ppm. The identity of this Ni(0) product has been established unequivocally through independent synthesis from Ni(COD)$_2$, 2 equiv. of PPh_3 and L′ in an NMR tube reaction under otherwise identical conditions.

IR spectra obtained with a dip probe at 193 K showed the appearance of an intense band at 2051 cm^{-1}, along with a weak band at 2152 cm^{-1}, for **5***2L′ whose intensity reached a maximum after the addition of 2 equiv. of L′. As expected, both bands disappeared upon warming the solution to room temperature due to the disproportionation of **5***2L′, and were replaced by broad bands at 2109 and 2060 cm^{-1}. These bands compare well with the literature reported values for complexes of the type $(Ph_3P)_n(RNC)_{4-n}$Ni(0), with n = 1–3, and R = ^{t}Bu, Cy, and $PhCH_2$.[63]

In clear contrast, addition of 1 equiv. of L′ to **3** at 213 K afforded an asymmetric compound which we assign as **6** shown in Scheme 5. The complete assignment of ^{1}H and ^{31}P NMR data of putative **6** is given in the ESI.† The PMe_3 ligands in **6** are non-equivalent but appear to coordinate to the same nickel site, with $^2J_{P-P}$ = |54| Hz.[64] The magnitude of $^3J_{P-P}$ of the putative isomeric structure $\mathbf{6}_{iso}$ may be expected to be significantly smaller if detectable at all.[20] Selective ^{31}P decoupling of ^{1}H NMR data aided in the assignment of the two PMe_3 ligands. Both phosphine ligands showed ^{1}H–^{1}H NOE contacts to L′ (δ_H 3.32 ppm), which would not have been possible if PMe_3 and L′ were coordinating in a *trans*-fashion to the same nickel ion as in $\mathbf{6}_{iso}$. Ni-arene d-π* back bonding appears to be insignificant, judging from the chemical shifts of the four distinct resonances of the central ring protons, δ_H being 7.74, 6.53, 6.47, and 6.18 ppm at 193 K. The central π-system of the 4-terphenyl backbone may act as a σ-donor to complete the ligand shell at the Ni–L′ site as indicated in Scheme 5. As observed for complex **2**, the shift of one of the above ^{1}H resonances to a lower field may reflect dative bonding of the π-system to nickel which binds another strong σ-donor ligand such as PCy_3 and L′ in the *trans*-position.

The structure of **6** is dynamic in solution. Exchange spectra show that the PMe_3 ligands slowly exchange Ni sites with L′ at

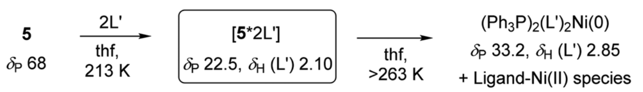

Scheme 4 Reactivity of binuclear **5** toward $CNCH_3$ (L′) monitored *in situ* by VT NMR spectroscopy in d_8-thf ($\delta_{Nucleus}$ in ppm at 11.7 T).

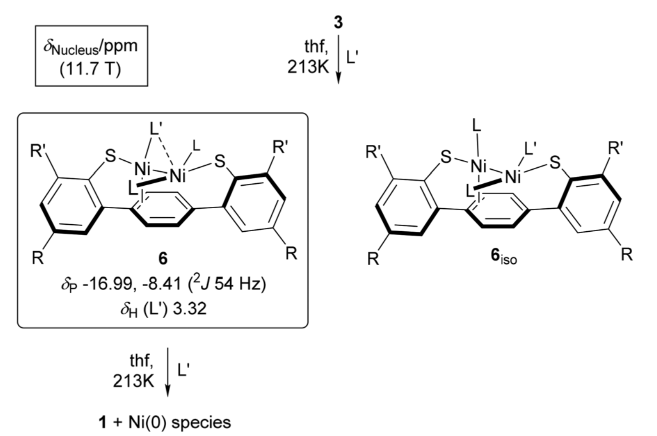

Scheme 5 Reactivity of **3** toward $CNCH_3$ (L′) monitored by *in situ* VT NMR spectroscopy (L = PMe_3, R′ = 2,4,6-$(H_3C)_3C_6H_2$, R = ^{t}Bu). Dashed line accounts for the capability of L′ to μ-bonding.

213 K, see Fig. S1 and S2 in the ESI.† The known capability of L′ to coordinate in a μ-fashion[19,65] likely triggers this exchange process as indicated in Scheme 5.

Monitoring the addition of L′ to **3** at 193 K in thf by IR spectroscopy showed the gradual appearance of a broad band at 2064 cm^{-1}, along with a significantly weaker broad band centred at 2124 cm^{-1}. Bands at wavenumbers greater than 2000 cm^{-1} have been reported as characteristic for terminal rather than bridging coordination of isocyanide ligands in binuclear complexes of low-valent nickel.[19,65] Compared to a reference sample with no added **3**, L′ coordination results in a shift of the C≡N stretching mode by 100 cm^{-1} to lower energy, indicating a significant d-π* charge transfer from Ni to L′. At 234 K, ^{1}H NMR resonances of the central arene ring protons are subject to exchange broadening and resonances of **1** began to gradually grow into the spectra. The addition of two equivalents of L′ to **3** resulted in complete conversion of **6** into **1**. IR spectra obtained at the same temperatures showed a broad band centred at 1855 cm^{-1} that irreversibly formed at the expense of the bands at 2124 and 2064 cm^{-1} that had originally been observed upon L′ addition at 193 K.

Conclusions

Mono- and binuclear complexes of Ni(I) have been prepared from a 4-terphenyldithiophenol ligand. Steric interactions between phosphine and substituents at the 4-terphenyl backbone result in the formation of coordination isomeric structures with thiolate bonding either in a bridging or terminal fashion. In the latter case, significant d-π* charge transfer causes the 4-terphenyl ligand backbone to coordinate to the Ni ions in a *syn*-μ-η^3:η^3 fashion. Electronic coupling of metal centres within the $Ni_2(\mu\text{-}S)_2$ core displayed in **4** and **5** involves bonding interactions *via* the bridging thiolates and also direct M–M bonding with calculated δ_5(Ni–Ni) = 0.548, whereas a delocalisation index of 0.225 indicates significantly weaker coupling of the Ni(I) ions in **3**. The origin of the chemical shift dependence on temperature observed for **3–5** is currently not understood but most likely reflects changes of the electronic properties of the bimetallic core. Whereas metal–thiolate bonding couples protons 3/5-H to the Ni ions, 8/9-H at the central π-system bind directly to the latter. Albeit plausible this hypothesis necessitates further studies.

Coordination of a π-acceptor ligand such as methyl isocyanide to **3** and **5** subjects the bimetallic fragments to disproportionation. Interestingly, the nature of the phosphine ligand determines the character of intermediately formed species and the temperature at which Ni(0) species are extruded. The binuclear $Ni_2(\mu\text{-}S)_2$ structure in **5** persists upon binding of 2 equiv. of isocyanide at low temperatures. In the case of **3**, apparent PMe_3 migration to the same nickel site is triggered by isocyanide bonding. This structural reorganisation reaction is remarkably facile even at low temperature which may be a consequence of the weak electronic coupling of the Ni ions, as also reflected by the calculated delocalisation index from solid state structural data.

The magnitude of metal–metal electronic coupling may be taken as a parameter which determines the electronic flexibility and thus the reactivity of bimetallic structures.[66] The bimetallic complexes of nickel described herein provide a complementary set of model compounds suitable for studies on the structural effects on the reactivity of binuclear systems toward electrophilic reactants.

Experimental

General considerations

All reactions were carried out under a dry argon atmosphere using standard Schlenk or glove box techniques (MBraun, MB 150-GI). All solvents were purified and dried prior to use. Dichloromethane and hexane were dried over Grubbs columns of a MBraun solvent purification system. Benzene, diethyl ether, pentane, tetrahydrofuran, and toluene were pre-dried over activated 3 Å molecular sieves and distilled from sodium benzophenone ketyl or potassium metal under argon. Methanol was dried over activated neutral alumina. d_6-Benzene, d_8-toluene, and d_8-thf were dried over and distilled from the NaK alloy whereas d-$CHCl_3$ and d_2-CH_2Cl_2 were dried over and vacuum transferred from 3 Å molecular sieves. All solvents were stored over 3 Å molecular sieves under argon. Molecular sieves and neutral alumina were activated by heating under dynamic vacuum (10^{-3} mbar) at 250 °C for 24–48 hours. UV-Vis spectra were collected on a PerkinElmer Lambda 35 spectrophotometer. The range from 200 to 1100 nm was scanned at a speed of 480 nm per minute, using 1 cm quartz cuvettes sealed with Teflon stoppers. Combustion analyses were performed on an Elementar Vario MICRO instrument. NMR data were recorded on Bruker Avance II 400 and DRX 250 instruments. VT NMR spectra were collected on a Bruker AVII+500 spectrometer. δ Values are given in ppm, J values in Hz. ^{1}H and ^{13}C{^{1}H} NMR chemical shifts are referenced to the residual proton and naturally abundant carbon resonances of the solvents: 7.16/128.06 (d_6-C_6H_6), 3.58/67.21 (d_8-thf), 5.32/53.84 (d_2-CH_2Cl_2), and 7.26/77.16 (d-$CHCl_3$) ppm. ^{31}P NMR chemical shifts are referenced to an external standard sample of 85% H_3PO_4 set to 0 ppm. VT solution IR spectra were obtained with a Mettler Toledo ReactIR 15 system equipped with a Sicomp dip probe at a spectral range from 2600 to 650 cm^{-1}. Ligand preparation is described in the ESI.† The compounds $(Me_3P)_2NiCl_2$,[67] $Ni(COD)_2$,[68] $(Ph_3P)_2NiN(SiMe_3)_2$,[69] $(pyridine)_4NiCl_2$,[70] and methyl isocyanide[71] were prepared following the procedures adapted from the literature. *Caution*: Methyl isocyanide is toxic and has a very unpleasant odour. All manipulations with this reagent should be carried out in a fume hood. X-ray data were collected on a Bruker Smart APEX II diffractometer with graphite-monochromated Mo K_α radiation. The programs used were Bruker's APEX2 v2011.8-0, including SADABS for absorption correction and SAINT for structure solution,[72] the WinGX suite of programs version

2013.3,[73] SHELXS for structure solution, SHELXL for structure refinement,[74,75] and PLATON.[76] Crystals were, unless otherwise noted, coated in a perfluorinated polyether oil and mounted on a 100 μm MiTeGen MicroMounts™ loop that was placed on the goniometer head under a stream of dry nitrogen at 100 K.

Preparation and characterization of 1

Ligand (500 mg, 0.776 mmol), benzyl potassium (210 mg, 1.550 mmol), and toluene (40 mL) were combined in a Schlenk flask. The resulting mixture was stirred for 0.5 hour (h) at room temperature (r.t.) to form a clear yellow solution. After this time, $(Me_3P)_2NiCl_2$ (220 mg, 0.780 mmol) was added and stirring was continued for an additional 2 h at r.t. The solution gradually turned dark purple and a white solid separated. The solid was filtered off, the solvent removed under vacuum, and the residual dark purple solid repeatedly (3×) washed with 10 mL portions of methanol, and dried under dynamic vacuum to produce a purple solid **1** (576 mg, 88%). Bulk crystallisation by slow diffusion of methanol layered on top of a concentrated solution of **1** in benzene produced single crystals also suitable for XRD analysis.

δ_H (400 MHz; d_6-C_6H_6; 298 K) 7.76 (2 H, d, J_{3-5} 2.4, 4, 3-, 18-H), 7.56 (4 H, s, 8-, 9-, 11-, 12-H), 7.05 (2 H, d, J_{5-3} 2.6, 4, 5-, 16-H), 6.95 (4 H, s, 21-, 23-, 32-, 34-H), 2.29 (12 H, s, 25-, 27-, 36-, 38-H), 2.17 (6 H, s, 26-, 37-H), 1.33 (18 H, s, 4-, and 17-^{t}Bu), 0.77 (18 H, *N*-line pattern $^{|2+4|}J_{H-P}$ 7.83, P(CH_3)$_3$).

δ_C (100 MHz; d_6-C_6H_6; 298 K) 144.22, 143.41, 141.83 (t, $\bar{J}_{C-P}$ 2.1, C-1, -14), 141.63 (C-19, -30), 140.75, 140.12, 136.10 (C-20, -24, -31, -35), 135.65 (C-22, -33), 128.36 (C-21, -23, -32, -34), 126.34 (C-5, -16), 123.85 (C-8, -9, -11, -12), 122.77 (C-3, -18), 34.19 (C-28, -40), 31.63 (C-29, -39), 21.19 (C-26, -37), 20.97 (C-25, -27, -36, -38), 12.47 (*N*-line pattern $^{|1+3|}J_{C-P}$ 27.7, P(CH_3)$_3$).

δ_P (162 MHz, d_6-C_6H_6, 298 K) −27.98 (Ni-*P*(CH_3)$_3$).

Elemental analysis found: C, 68.26; H, 8.35; S, 6.73. Calc. for $C_{50}H_{66}P_2S_2\cdot2CH_3OH$: C, 68.18; H, 8.16; S, 7.00%.

UV-Vis: λ_{max} (thf) nm 257 (ε/dm^3 mol^{-1} cm^{-1} 67 671), 280 (52 736), 351 (13 220) and 511 (1128).

Crystal data: $C_{50}H_{66}P_2S_2\cdot2CH_3OH$, M = 915.88, monoclinic, a = 13.5105(2), b = 12.1898(2), c = 29.9385(5) Å, U = 4928.25(14) Å^3, T = 100(2) K, space group $P121/c$, Z = 4, 27715 reflections measured, 10 728 unique (R_{int} = 0.0223) which were used in all calculations. The final w$R(F_2)$ was 0.1114 (all data).

Preparation and characterization of 3

1 (200 mg, 0.234 mmol), Ni(COD)$_2$ (65 mg, 0.234 mmol), and thf (25 mL) were combined in a Schlenk flask. The resulting mixture was stirred for 2 h at r.t. to form a brown solution. The solvent was removed under vacuum, and the residual brown solid repeatedly washed with 5 ml portions of pentane (3×), and dried under dynamic vacuum to produce a brown solid **3** (110 mg, 51%). Slow evaporation of a concentrated solution of **3** in pentane produced single crystals suitable for XRD analysis. Further purification was carried out by cooling a saturated solution of **3** (200 mg) in diethyl ether/pentane (1 : 1) to 238 K to yield brown crystals of **3** (110 mg, 55%). Prolonged evacuation of solid **3** must be avoided since concomitant removal of volatile PMe_3 leads to gradual sample degradation.

δ_H (500 MHz, d_8-thf, 178 K) 7.29 (2 H, d, J_{3-5} 1.7, 4, 3-, 18-H), 6.87 (2 H, d, J_{5-3} 1.7, 4, 5-, 16-H), 6.83 (4 H, s, 21-, 23-, 32-, 34-H), 5.59 (2 H, br s), 4.97 (2 H, br s), 2.28 (6 H, s, 26-, 37-H), 1.95 (12 H, s, 25-, 27-, 36-, 38-H), 1.33 (18 H, s, 4-, and 17-^{t}Bu), 1.29 and 1.28 (s, P(CH_3)$_3$).

δ_C (126 MHz, d_8-thf, 178 K) 152.42 (C-1, -14), 144.05, 140.80, 139.03 (C-19, -30), 136.00, 135.34, 134.81, 127.53 (C-21, -23, -32, -34), 125.75 (C-5, -16), 122.21 (C-3, -18), 109.43, 98.51, 74.23, 34.12 (C-28, -40), 31.11 (C-29, -39), 20.5 (C-25, -27, -36, and -38), 20.5 (C-26, -37), 15.72 (J_{C-7-P} 26.5, P(CH_3)$_3$).

δ_P (202 MHz, d_8-thf, 178 K) −13.66.

Elemental analysis found: C, 66.08; H, 7.45; S, 6.83. Calc. for $C_{50}H_{66}S_2$: C, 65.96; H, 7.31; S, 7.04%.

UV-Vis: λ_{max} (thf)/nm 266 (ε/dm^3 mol^{-1} cm^{-1} 25 089), 328 (20 496), 373 (15 074), 520 (2044) and 943 (310).

Crystal data: $C_{50}H_{66}Ni_2P_2S_2\cdot C_5H_{12}$, M = 982.65, monoclinic, a = 15.8803(8), b = 20.1160(10), c = 17.6539(9) Å, U = 5371.9(5) Å^3, T = 100(2) K, space group $P121/n$, Z = 4, 75839 reflections measured, 15 591 unique (R_{int} = 0.0321) which were used in all calculations. The final w$R(F_2)$ was 0.1389 (all data).

Preparation and characterization of 2

Ligand (500 mg, 0.776 mmol), benzyl potassium (210 mg, 1.550 mmol), and toluene (40 mL) were combined in a Schlenk flask. The resulting mixture was stirred for 30 minutes at r.t. to form a clear yellow solution. After (pyridine)$_4$NiCl$_2$ (360 mg, 0.776 mmol) and tricyclohexylphosphine (210 mg, 0.776 mmol) were added, stirring was continued for an additional 2 h at r.t. The solution turned brown and a white solid separated. After filtration, the solvent was removed under vacuum, the residual brown solid repeatedly (3×) washed with 10 mL portions of methanol, and dried under dynamic vacuum to produce a dark purple solid **2** (456 mg, 60%). Crystallisation by slow diffusion of pentane vapour into a concentrated solution of **2** in thf produced single crystals suitable for XRD analysis.

δ_H (500 MHz; d_2-CH_2Cl_2; 273 K) 7.76 (4 H, s, 8-, 9-, 11-, 12-H), 7.27 (2 H, d, J_{3-5} 2.3, 4, 3-, 18-H), 6.78 (4 H, s, 21-, 23-, 32-, 34-H), 6.73 (2 H, d, J_{5-3} 2.3, 4, 5-, 16-H), 2.19 (6 H, s, 26-, 37-H), 1.91 (12 H, s, 25-, 27-, 36-, 38-H), 1.27 (18 H, s, 4-, and 17-^{t}Bu), 2.04–0.75 (m, P(C_6H_{11})$_3$).

δ_C (126 MHz; d_2-CH_2Cl_2; 273 K) 146.25 (C-4, -17), 141.72 (C-6, -15), 141.02 (C-19, -30), 140.71 (C-2, -13), 139.60 (C-7, -10), 137.93 (C-1, -14), 136.07 (C-20, -24, -31, -35), 135.88 (C-22, -33), 128.08 (C-21, -23, -32, -34), 127.59 (C-5, -16), 121.49 (C-3, -18), 118.62 (C-8, -9, -11, -12), 34.56 (C-28, -40), 33.53 (d, P(C_6H_{11})$_3$), 31.42 (C-29, -39), 30.11 (d, P(C_6H_{11})$_3$), 27.19 (d, P(C_6H_{11})$_3$), 26.82 (d, P(C_6H_{11})$_3$), 21.15 (C-26, -37), 20.88 (C-25, -27, -36, -38).

δ_P (162 MHz, d_2-CH_2Cl_2, 273 K) 15.42.

Elemental analysis found: C, 74.32; H, 8.44; S, 6.27. Calc. for $C_{62}H_{81}S_2$: C, 75.98; H, 8.33; S, 6.54%.

UV-Vis: λ_{max} (thf)/nm 253 (ε/dm^3 mol^{-1} cm^{-1} 28 630), 269 (27 354), 283 (24 012), 298 (21 892), 453 (4545) and 550 (3545).

Crystal data: $C_{62}H_{81}NiPS_2 \cdot C_4H_8O$, M = 1052.17, monoclinic, a = 9.7947(5), b = 31.5469(16), c = 19.7427(11) Å, U = 6084.0(6) Å^3, T = 100(2) K, space group $P121/n$, Z = 4, 81 481 reflections measured, 12 065 unique (R_{int} = 0.0491) which were used in all calculations. The final w$R(F_2)$ was 0.2111 (all data).

Preparation and characterization of 4

Compound **2** (100 mg, 0.102 mmol), $Ni(COD)_2$ (28 mg, 0.102 mmol), tricyclohexylphosphine (29 mg, 0.103 mmol), and thf (25 mL) were combined in a Schlenk flask. The resulting mixture was stirred for 2 h at r.t. to form a yellow solution. After removing the solvent under dynamic vacuum, the residual yellow solid was repeatedly (3×) washed with 5 mL portions of pentane, and dried under dynamic vacuum to produce solid yellow **4** (80 mg, 75%). Bulk crystallisation by slow diffusion of pentane layered on top of a concentrated thf solution produced single crystals suitable for XRD analysis.

δ_H (500 MHz, d_8-thf, 253 K) 8.59 (4 H, br s, 8-, 9-, 11-, 12-H), 7.35 (2 H, d, J_{3-5} 2.3, 4, 3-, 18-H), 6.81 (2 H, d, J_{5-3} 2.2, 4, 5-, 16-H), 6.74 (4 H, s, 21-, 23-, 32-, 34-H), 2.23 (6 H, s, 26-, 37-H), 1.94 (12 H, s, 25-, 27-, 36-, 38-H), 1.30 (18 H, s, 4-, and 17-^{t}Bu), 2.05–0.72 ($P(C_6H_{11})_3$).

δ_C (126 MHz, d_8-thf, 253 K) 164.86 (C-2, -13), 150.45 (C-6, -15), 146.71 (C-4, -17), 143.19 (C-7, -10), 141.81 (C-19, -30), 139.52 (C-1, -14), 136.32 (C-20, -24, -31, -35), 135.47 (C-22, -33), 127.75 (C-21, -23, -32, -34), 126.30 (C-5, -16), 124.95 (C-8, -9, -11, -12), 121.56 (C-3, -18), 35.92 (PCy_3), 34.88 (C-28, -40), 31.47 (C-29, -39), 30.63 (PCy_3), 28.10 (PCy_3), 27.20 (PCy_3), 23.08 (C-25, -27, -36, -38), 21.12 (C-26, -37).

δ_P (202 MHz, d_8-thf, 253 K): 35 ($\nu_{1/2} \sim$ 5000 Hz).

Elemental analysis found: C, 72.28; H, 8.74; S, 4.60. Calc. for $C_{80}H_{114}S_2$: C, 72.84; H, 8.71; S, 4.86%.

UV-Vis: λ_{max} (thf)/nm 220 (ε/dm^3 mol^{-1} cm^{-1} 15 789), 248 (25 725), 311 (6257), 352 (3005), 789 (233) and 972 (227).

Crystal data: $C_{80}H_{114}Ni_2P_2S_2$, M = 1319.19, triclinic, a = 11.1421(4), b = 12.9165(5), c = 26.8959(10) Å, T = 130(2) K, space group $P\bar{1}$, Z = 2, 51 911 reflections measured, 17 549 unique (R_{int} = 0.0224) which were used in all calculations. The final w$R(F_2)$ was 0.1013 (all data).

Preparation and characterization of 5

To a yellow solution of $(Ph_3P)_2NiN(SiMe_3)_2$ (463 mg, 0.622 mmol) in thf (50 mL) was added a solution of the ligand (200 mg, 0.311 mmol) in thf (5 mL) dropwise, and the resulting mixture stirred for 2 h at r.t. The solution gradually turned dark green. After removing the solvent under dynamic vacuum, the residual green solid was repeatedly (3×) washed with 10 mL portions of pentane, and dried under dynamic vacuum to produce solid **5** (215 mg). The raw product contains additional PPh_3, typically ≤5%, as the only impurity. NMR spectroscopic properties of raw products are identical to samples recovered after one and two recrystallization steps. Recrystallization was performed by slow vapour diffusion of pentane, or hexane, into a concentrated solution of **5** in thf and produced green single crystals which were also suitable for XRD analysis (155 mg 39%). Other than the co-crystallized hydrocarbon, the material contains varying amounts of trapped thf, rendering elemental analysis difficult.

δ_H (500 MHz, d_6-C_6H_6, 299 K) 12.01 (4 H, br s, 8-, 9-, 11-, 12-H), 7.99 (2 H, d, J_{3-5} 1.6, 4, 3-, 18-H), 7.86 (2 H, d, J_{5-3} 1.8, 4, 5-, 16-H), 7.48 (m, PPh_3), 7.02 (m, PPh_3), 6.84 (m, PPh_3), 6.78 (4 H, s, 21-, 23-, 32-, 34-H), 2.28 (6 H, s, 26-, 37-H), 1.68 (12 H, s, 25-, 27-, 36-, 38-H), 1.22 (18 H, s, 4-, and 17-^{t}Bu).

δ_C (126 MHz, d_6-C_6H_6, 299 K) 164.71, 152.34, 142.79, 136.41, 136.37, 135.04, 133.70, 129.49, 128.02, 126.01, 115.33, 33.20, 32.25, 21.27, 20.73.

δ_H (500 MHz, d_8-thf, 298 K) 10.12 (4 H, br s, 8-, 9-, 11-, 12-H), 7.53 (2 H, d, J_{3-5} 2.2, 4, 3-, 18-H), 7.36 (2 H, d, J_{5-3} 2.3, 4, 5-, 16-H), 7.29 (m, PPh_3), 7.17 (m, PPh_3), 6.55 (4 H, s, 21-, 23-, 32-, 34-H), 2.26 (6 H, s, 26-, 37-H), 1.36 (18 H, s, 4-, and 17-^{t}Bu), 1.26 (12 H, s, 25-, 27-, 36-, 38-H).

δ_C (126 MHz, d_8-thf, 298 K) 159.11, 150.80 (C-4, -17), 147.85, 142.56 (C-19, -30), 137.45, 137.09 (PPh_3), 136.05, 135.47 (PPh_3), 130.58 (C-8, -9, -11, -12), 130.09 (PPh_3), 129.24, 128.80 (PPh_3), 128.23 (C-21, -23, -32, -34), 127.73 (C-5, -16), 125.60 (C-1, -14), 124.93 (C-3, -18), 34.57 (C-28, -40), 32.39 (C-29, -39), 21.60 (C-25, -27, -36, -38), 21.10 (C-26, -37).

δ_P (202 MHz, d_8-thf, 213 K) 68 ($\nu_{1/2} \sim$ 800 Hz).

Elemental analysis found: C, 73.84; H, 6.22; S, 4.87. Calc. for $C_{80}H_{78}S_2$: C, 74.90; H, 6.13; S, 5.00%.

UV-Vis: λ_{max} (thf)/nm 315 (ε/dm^3 mol^{-1} cm^{-1} 13 205), 380 (17 718), 450 (7821), 725 (576) and 990 (527).

Crystal data: $C_{80}H_{78}Ni_2P_2S_2$, M = 1282.9, triclinic, a = 11.9127(3), b = 21.1860(5), c = 28.2328(7) Å, T = 100(2) K, space group $P\bar{1}$, Z = 4, 275458 reflections measured, 30 564 unique (R_{int} = 0.0235) which were used in all calculations. The final w$R(F_2)$ was 0.0936 (all data).

Computational details

DFT calculations of **3** and **5** were performed using the Gaussian 09 program suite,[42] using the B3LYP density functional,[43–45] along with the implemented 6-311G(d,p) basis set[46–49] and dispersion corrections, including Becke–Johnson damping.[50,51] For the theoretical model systems, the ^{t}Bu substituents on the bridging 4-terphenyldithiophenolate ligand were replaced by methyl groups. All geometry optimizations were initially carried out without imposing any symmetry constraints. The geometry of **3**, however, converged close to C_2 symmetry and was subsequently optimised within this symmetry. All geometrical parameters were in excellent agreement with their experimental counterparts. The optimized structures were confirmed as true minima on the respective potential energy surface by calculating analytical frequencies. Modes with imaginary frequencies were absent for both **3** and **5**. The topology of the electron density was analysed using the software package Aimall.[41] Plots were generated using Aimall and Chemcraft.[77]

Acknowledgements

This work was funded by the Fonds der Chemischen Industrie, FCI, in the form of a Liebig scholarship to A.B. which includes a doctoral scholarship to F.K. We thank Prof. Rainer Winter and Stefan Scheerer, University of Konstanz, for helpful discussions and Dr Klaus Eichele for assistance with and discussion of NMR data. Umicore AG & Co. KG, Hanau, Germany is acknowledged for the generous donation of $(^{t}Bu_3P)_2Pd$.

Notes and references

1 K. T. Horak, A. Velian, M. W. Day and T. Agapie, *Chem. Commun.*, 2014, **50**, 4427–4429.
2 J. Wu, A. Nova, D. Balcells, G. W. Brudvig, W. Dai, L. M. Guard, N. Hazari, P.-H. Lin, R. Pokhrel and M. K. Takase, *Chem. – Eur. J.*, 2014, **20**, 5327–5337.
3 R. Beck and S. A. Johnson, *Organometallics*, 2013, **32**, 2944–2951.
4 S. T. Chao, N. C. Lara, S. Lin, M. W. Day and T. Agapie, *Angew. Chem., Int. Ed.*, 2011, **50**, 7529–7532.
5 C. Jones, C. Schulten, L. Fohlmeister, A. Stasch, K. S. Murray, B. Moubaraki, S. Kohl, M. Z. Ertem, L. Gagliardi and C. J. Cramer, *Chem. – Eur. J.*, 2011, **17**, 1294–1303.
6 A. L. Keen and S. A. Johnson, *J. Am. Chem. Soc.*, 2006, **128**, 1806–1807.
7 G. Bai, P. Wei and D. W. Stephan, *Organometallics*, 2005, **24**, 5901–5908.
8 J. J. Schneider, D. Wolf, U. Denninger, R. Goddard and C. Krüger, *J. Organomet. Chem.*, 1999, **579**, 139–146.
9 D. Adhikari, S. Mossin, F. Basuli, B. R. Dible, M. Chipara, H. Fan, J. C. Huffman, K. Meyer and D. J. Mindiola, *Inorg. Chem.*, 2008, **47**, 10479–10490.
10 R. Beck, M. Shoshani, J. Krasinkiewicz, J. A. Hatnean and S. A. Johnson, *Dalton Trans.*, 2013, **42**, 1461–1475.
11 M. Ito, T. Matsumoto and K. Tatsumi, *Inorg. Chem.*, 2009, **48**, 2215–2223.
12 A. Mondragón, M. Flores-Alamo, P. R. Martínez-Alanis, G. Aullón, V. M. Ugalde-Saldívar and I. Castillo, *Inorg. Chem.*, 2015, **54**, 619–627.
13 D. A. Vicic and W. D. Jones, *J. Am. Chem. Soc.*, 1997, **119**, 10855–10856.
14 B. R. Dible, M. S. Sigman and A. M. Arif, *Inorg. Chem.*, 2005, **44**, 3774–3776.
15 A. Velian, S. Lin, A. J. M. Miller, M. W. Day and T. Agapie, *J. Am. Chem. Soc.*, 2010, **132**, 6296–6297.
16 Y.-Y. Zhou, D. R. Hartline, T. J. Steiman, P. E. Fanwick and C. Uyeda, *Inorg. Chem.*, 2014, **53**, 11770–11777.
17 C. A. Laskowski and G. L. Hillhouse, *Organometallics*, 2009, **28**, 6114–6120.
18 K. Jonas and G. Wilke, *Angew. Chem., Int. Ed. Engl.*, 1970, **9**, 312–313.
19 G. M. Ferrence, E. Simón-Manso, B. K. Breedlove, L. Meeuwenberg and C. P. Kubiak, *Inorg. Chem.*, 2004, **43**, 1071–1081.
20 A. Miedaner and D. L. DuBois, *Inorg. Chem.*, 1988, **27**, 2479–2484.
21 J. J. Eisch, A. M. Piotrowski, K. I. Han, C. Kruger and Y. H. Tsay, *Organometallics*, 1985, **4**, 224–231.
22 R. Beck and S. A. Johnson, *Chem. Commun.*, 2011, **47**, 9233–9235.
23 U. Denninger, J. J. Schneider, G. Wilke, R. Goddard and C. Krüger, *Inorg. Chim. Acta*, 1993, **213**, 129–140.
24 J. J. Schneider, U. Denninger, J. Hagen, C. Krüger, D. Bläser and R. Boese, *Chem. Ber.*, 1997, **130**, 1433–1440.
25 O. Jarchow, H. Schulz and R. Nast, *Angew. Chem., Int. Ed. Engl.*, 1970, **9**, 71.
26 G. Wilke, *Angew. Chem., Int. Ed. Engl.*, 1988, **27**, 185–206.
27 C. A. Laskowski and G. L. Hillhouse, *Chem. Sci.*, 2011, **2**, 321–325.
28 T. J. Steiman and C. Uyeda, *J. Am. Chem. Soc.*, 2015, **137**, 6104–6110.
29 P. J. Blower and J. R. Dilworth, *Coord. Chem. Rev.*, 1987, **76**, 121–185.
30 D. W. Stephan and T. Timothy Nadasdi, *Coord. Chem. Rev.*, 1996, **147**, 147–208.
31 E. Bouwman and J. Reedijk, *Coord. Chem. Rev.*, 2005, **249**, 1555–1581.
32 P. Kilian, F. R. Knight and J. D. Woollins, *Coord. Chem. Rev.*, 2011, **255**, 1387–1413.
33 J. C. Bayón, C. Claver and A. M. Masdeu-Bultó, *Coord. Chem. Rev.*, 1999, **193–195**, 73–145.
34 E. I. Solomon, S. I. Gorelsky and A. Dey, *J. Comput. Chem.*, 2006, **27**, 1415–1428.
35 D. Sellmann and J. Sutter, *Acc. Chem. Res.*, 1997, **30**, 460–469.
36 H. Wadepohl, *Angew. Chem., Int. Ed. Engl.*, 1992, **31**, 247–262.
37 T. Murahashi, K. Takase, M.-a. Oka and S. Ogoshi, *J. Am. Chem. Soc.*, 2011, **133**, 14908–14911.
38 A. Falceto, D. Casanova, P. Alemany and S. Alvarez, *Chem. – Eur. J.*, 2014, **20**, 14674–14689.
39 The longer Ni–C distance of 256.5(2) pm found for the second crystallographically independent formula unit results from packing effects between the C_6H_5 rings of the respective PPh_3 ligands. See the ESI† for details.
40 R. F. Bader, *Atoms in molecules : a quantum theory*, Clarendon Pr., Oxford, 1990.
41 T. A. Keith, *AIMALL, TK Gristmill Software*, Overland Park KS, USA, 2014, aim.tkgristmill.com.
42 M. J. Frisch, G. W. Trucks, H. B. Schlegel, G. E. Scuseria, M. A. Robb, J. R. Cheeseman, G. Scalmani, V. Barone, B. Mennucci, G. A. Petersson, H. Nakatsuji, M. Caricato, X. Li, H. P. Hratchian, A. F. Izmaylov, J. Bloino, G. Zheng, J. L. Sonnenberg, M. Hada, M. Ehara, K. Toyota, R. Fukuda, J. Hasegawa, M. Ishida, T. Nakajima, Y. Honda, O. Kitao, H. Nakai, T. Vreven, J. A. Montgomery Jr., J. E. Peralta, F. Ogliaro, M. J. Bearpark, J. Heyd, E. N. Brothers, K. N. Kudin, V. N. Staroverov, R. Kobayashi, J. Normand, K. Raghavachari, A. P. Rendell, J. C. Burant, S. S. Iyengar, J. Tomasi, M. Cossi, N. Rega, N. J. Millam, M. Klene, J. E. Knox, J. B. Cross, V. Bakken, C. Adamo, J. Jaramillo,

R. Gomperts, R. E. Stratmann, O. Yazyev, A. J. Austin, R. Cammi, C. Pomelli, J. W. Ochterski, R. L. Martin, K. Morokuma, V. G. Zakrzewski, G. A. Voth, P. Salvador, J. J. Dannenberg, S. Dapprich, A. D. Daniels, Ö. Farkas, J. B. Foresman, J. V. Ortiz, J. Cioslowski and D. J. Fox, *Gaussian 09*, Gaussian, Inc., Wallingford, CT, USA, 2009.
43 A. D. Becke, *J. Chem. Phys.*, 1993, **98**, 5648–5652.
44 C. Lee, W. Yang and R. G. Parr, *Phys. Rev. B: Solid State*, 1988, **37**, 785–789.
45 B. Miehlich, A. Savin, H. Stoll and H. Preuss, *Chem. Phys. Lett.*, 1989, **157**, 200–206.
46 A. D. McLean and G. S. Chandler, *J. Chem. Phys.*, 1980, **72**, 5639–5648.
47 R. Krishnan, J. S. Binkley, R. Seeger and J. A. Pople, *J. Chem. Phys.*, 1980, **72**, 650–654.
48 A. J. H. Wachters, *J. Chem. Phys.*, 1970, **52**, 1033–1036.
49 K. Raghavachari and G. W. Trucks, *J. Chem. Phys.*, 1989, **91**, 1062–1065.
50 S. Grimme, J. Antony, S. Ehrlich and H. Krieg, *J. Chem. Phys.*, 2010, **132**, 154104.
51 S. Grimme, S. Ehrlich and L. Goerigk, *J. Comput. Chem.*, 2011, **32**, 1456–1465.
52 L. J. Farrugia, C. Evans, H. M. Senn, M. M. Hänninen and R. Sillanpää, *Organometallics*, 2012, **31**, 2559–2570.
53 L. J. Farrugia and P. Macchi, *Struct. Bonding*, 2012, **146**, 127–158.
54 R. F. W. Bader, *J. Phys. Chem. A*, 1998, **102**, 7314–7323.
55 The BCP represents the point of minimum electron density, $\rho(\mathbf{r})$, along the bond path between two atoms, in which $\rho(\mathbf{r})$ is locally greater than in any direction away from the path.
56 P. Macchi and A. Sironi, *Coord. Chem. Rev.*, 2003, **238–239**, 383–412.
57 D. Cremer and E. Kraka, *Angew. Chem., Int. Ed. Engl.*, 1984, **23**, 627–628.
58 X. Fradera, M. A. Austen and R. F. W. Bader, *J. Phys. Chem. A*, 1998, **103**, 304–314.
59 S. Pfirrmann, C. Limberg, C. Herwig, C. Knispel, B. Braun, E. Bill and R. Stösser, *J. Am. Chem. Soc.*, 2010, **132**, 13684–13691.
60 R. Beck, M. Shoshani and S. A. Johnson, *Angew. Chem., Int. Ed.*, 2012, **51**, 11753–11756.
61 D. F. Evans, *J. Chem. Soc.*, 1959, 2003–2005.
62 C. Piguet, *J. Chem. Educ.*, 1997, **74**, 815.
63 E. Wenschuh, D. Wilhelm, H. Hartung and U. Baumeister, *Z. Anorg. Allg. Chem.*, 1994, **620**, 2048–2052.
64 D. J. Elliot, D. G. Holah, A. N. Hughes, H. A. Mirza and E. Zawada, *J. Chem. Soc., Chem. Commun.*, 1990, 32–33.
65 D. L. DeLaet, P. E. Fanwick and C. P. Kubiak, *Organometallics*, 1986, **5**, 1807–1811.
66 P. J. Hay, J. C. Thibeault and R. Hoffmann, *J. Am. Chem. Soc.*, 1975, **97**, 4884–4899.
67 O. Dahl, *Acta Chem. Scand.*, 1969, **23**, 2342–2354.
68 D. J. Krysan and P. B. Mackenzie, *J. Org. Chem.*, 1990, **55**, 4229–4230.
69 D. C. Bradley, M. B. Hursthouse, R. J. Smallwood and A. J. Welch, *J. Chem. Soc., Chem. Commun.*, 1972, 872–873.
70 S. M. Nelson and T. M. Shepherd, *J. Chem. Soc.*, 1965, 3276–3284.
71 R. E. Schuster, J. E. Scott and J. Casanova Jr., *Org. Synth.*, 1966, **46**, 75–77.
72 APEX2, Bruker AXS Inc., v 2011.8–0.
73 L. J. Farrugia, *J. Appl. Crystallogr.*, 1999, **32**, 837.
74 G. M. S. C. B. Hübschle and B. Dittrich, *J. Appl. Crystallogr.*, 2011, **44**, 1281–1284.
75 G. M. Sheldrick, *Acta Crystallogr., Sect. A: Fundam. Crystallogr.*, 2008, **64**, 112–122.
76 A. L. Speck, *Acta Crystallogr., Sect. D: Biol. Crystallogr.*, 2009, **65**, 148–155.
77 G. A. Zhurko, *CHEMCRAFT*, chemcraft.com.